

**NPL REPORT MAT 118**

**MICRO-CANTILEVER TESTING OF ENGINEERING COATINGS**

**HELEN JONES AND MARK GEE**

**JUNE 2023**



## **Micro-Cantilever Testing of Engineering Coatings**

Helen Jones and Mark Gee

Department of Materials and Mechanical Metrology

### **ABSTRACT**

The feasibility of using micro-mechanical testing of small cantilevers micro-machined from coated samples was explored. Two types of samples were fabricated. Cantilevers from a sample with a thin (few micrometre) TiN coating were fabricated with the cantilevers parallel to the surface of the coating. Cantilevers from a sample with a thick (50 micrometres) W based coating were fabricated with the interface at the base (highest stress position) of the cantilever. All the cantilevers were tested in situ in the SEM using an in situ nanoindenter to load the end of the cantilever. Load displacement curves were captured for all the tests and the measured cantilever geometry was used to calculate stress strain curves. Variability in results was shown for all the tests due to variation in cantilever geometry and microstructural effects. Interfacial failure was seen for only one of the cantilevers testing the interface in the W based coating with the rest showing significant plastic deformation.

© NPL Management Limited, 2023

ISSN 1754-2979

<https://doi.org/10.47120/npl.MAT118>

National Physical Laboratory

Hampton Road, Teddington, Middlesex, TW11 0LW

This work was funded by the UK Government's Department for Science, Innovation & Technology through the UK's National Measurement System programmes.

Extracts from this report may be reproduced provided the source is acknowledged and the extract is not taken out of context.

Approved on behalf of NPLML by  
Stefanos Giannis, Science Area Leader Advanced Engineering Materials

## CONTENTS

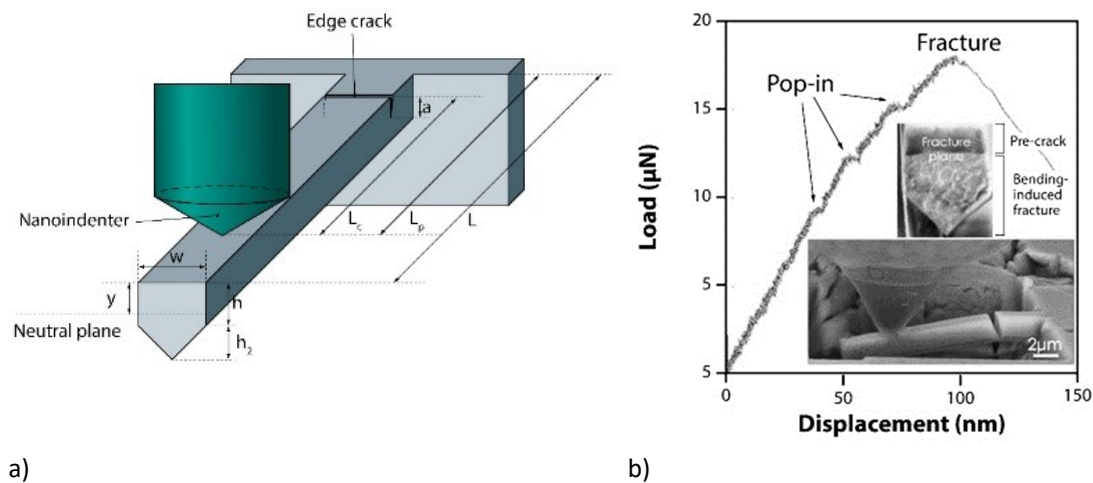
|          |                                                             |           |
|----------|-------------------------------------------------------------|-----------|
| <b>1</b> | <b>BACKGROUND.....</b>                                      | <b>1</b>  |
| <b>2</b> | <b>MATERIALS AND TEST METHODS .....</b>                     | <b>3</b>  |
| 2.1      | MATERIALS.....                                              | 3         |
| 2.2      | FIB MICROCANTILEVER FABRICATION.....                        | 10        |
| 2.2.1    | TiN cohesive strength cantilever.....                       | 10        |
| 2.2.2    | W based coating interface strength cantilever samples ..... | 11        |
| 2.3      | MICROCANTILEVER TESTING .....                               | 11        |
| <b>3</b> | <b>RESULTS.....</b>                                         | <b>12</b> |
| 3.1      | TIN COHESIVE STRENGTH CANTILEVERS .....                     | 12        |
| 3.2      | W BASED INTERFACE STRENGTH CANTILEVERS .....                | 13        |
| <b>4</b> | <b>DISCUSSION.....</b>                                      | <b>13</b> |
| <b>5</b> | <b>CONCLUSIONS.....</b>                                     | <b>16</b> |
| <b>6</b> | <b>ACKNOWLEDGEMENTS.....</b>                                | <b>16</b> |
| <b>7</b> | <b>REFERENCES.....</b>                                      | <b>16</b> |



## 1 BACKGROUND

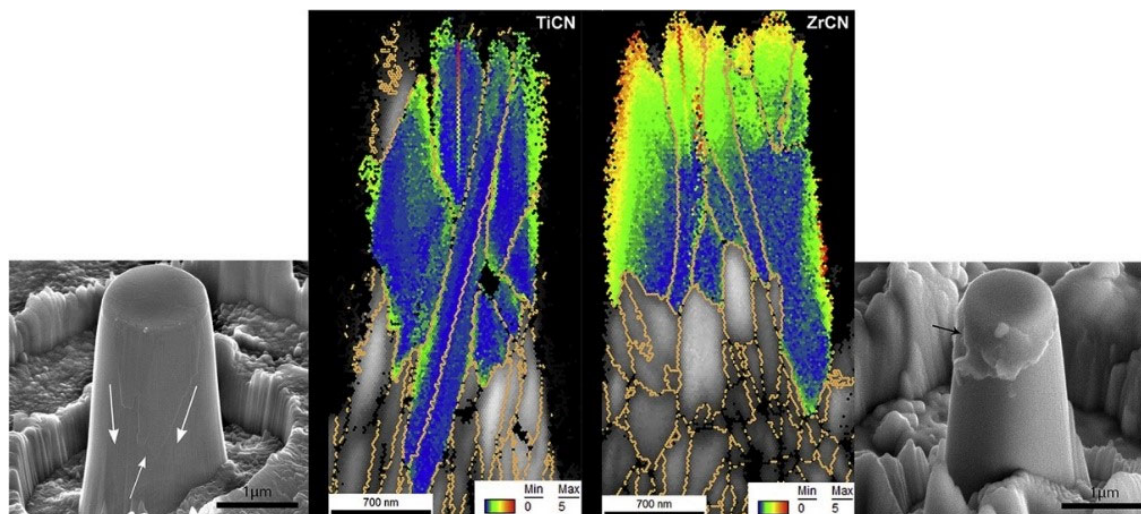
Micro-mechanical testing makes use of focused ion beam instruments (FIB) [1] that can be used to machine specimens with a resolution of a few 10s of nanometres. This creates regions of a sample that can be tested mechanically to measure properties of the coatings. Different specimen geometries can be created, such as pillars and cantilevers, which can be tested in different ways to measure different properties such as cohesive strength, interfacial strength and fracture toughness. The testing can be done ex situ or in situ depending on what data is required, where in situ testing also produces real-time imaging of the test specimen simultaneous with the mechanical data acquisition.

There are only a few studies of coatings using micromechanical testing, however some studies deposited the coating material directly into the test specimen geometry using the FIB and measured the mechanical properties [2], which would be likely different to an existing coating made from the same material. A more typical experiment, by fabricating cantilevers in a TBC [3] measured properties such as the elastic modulus, fracture toughness and flexural strength of the coating by analysing the load-deflection curve. The cantilevers can be positioned on the surface of the coating and through the layers, to evaluate the strength of different interfaces and grain boundaries, as shown in a recent study of APS TBC Figure 1 [4]. Finally, a study on thermal spray coatings (HVOF) [5] used SEM imaging of the cantilevers post-test to identify different fracture modes.



**Figure 1: Fracture toughness measurement of a TBC coating determined using a micromechanical test on a cantilever machined from the coating with a notch at the base of the cantilever, a) principle, b) images and results [4]**

Two studies using fabrication of pillars for ceramic coatings [5,6] used pillar splitting to look at fracture properties by indenting the top of the sample until cracks formed from the indent corners and down the pillar. The study on Cr-based coatings fabricated the pillars through a boundary [6] and did compression testing to investigate the mechanical failure of the interface. Pillar testing can also be combined with microstructural assessment to give information on the deformation mechanisms that have occurred (Figure 2) [7].



**Figure 2, Micromechanical samples machined from coatings and then sectioned and examined with EBSD analysis. On left TiCN and on right ZrCN [7].**

Although micro-mechanical testing provides a way of accessing several of the properties of coatings directly there are some drawbacks. Firstly, the scale of the stressed volume in these machined samples is small, so the need for a representative volume element, where the sample is true to the performance of the coating, needs to be considered carefully. Therefore, the mechanical behaviour becomes more dependent on the local microstructure than the bulk material, for example when test specimens contain only a few features, such as grains or pores. If the mechanical properties of the test specimens are dependent on the presence of defects, such as porosity or cracks, in the volume of the test specimen, then the statistical likelihood of these defects in the small volume may also affect results. Similarly, it is well known that small volumes of material can be stronger than larger volumes when normalised to the volume of material.

Secondly, the preparation of these small geometries by FIB can be complex. There are usually geometrical inaccuracies in the dimensions that deviate from the target geometry, meaning full analysis of the results requires finite element modelling of the real geometry. These inaccuracies include rounding at the edge of the specimens, tapering, and ion implantation from the FIB processing itself, all of which cause uncertainty in the measured mechanical properties of the specimen and material. Additionally, the pillar geometry is fixed at the base, thereby making Young's modulus impossible to measure due to non-uniform stress and strain down the pillar, therefore only a relative elastic modulus value is possible to measure.

The advantages of using micromechanical testing specifically for coatings are that a few micrometres on the surface are inspected, and often the total thickness of coatings is of the order of a few micrometres. This means that the mechanical properties of the coating can be isolated and measured without the effect of the substrate material. If the coating is multi-layered, it may be possible that individual layers can also be individually tested.

Investigating the mechanical properties of individual components within the coating also includes tests that isolate single interfaces, either within the coating or between the coating and substrate. These tests enable measurement of both cohesive and adhesive strengths of the coating.



If the tests are carried out in situ then an additional benefit of this is that the deformation and failure can be observed as it happens. This provides insight into fracture origin, early deformation processes and enables the corresponding mechanical data to be directly compared with the imaging at any point during the test.

## 2 MATERIALS AND TEST METHODS

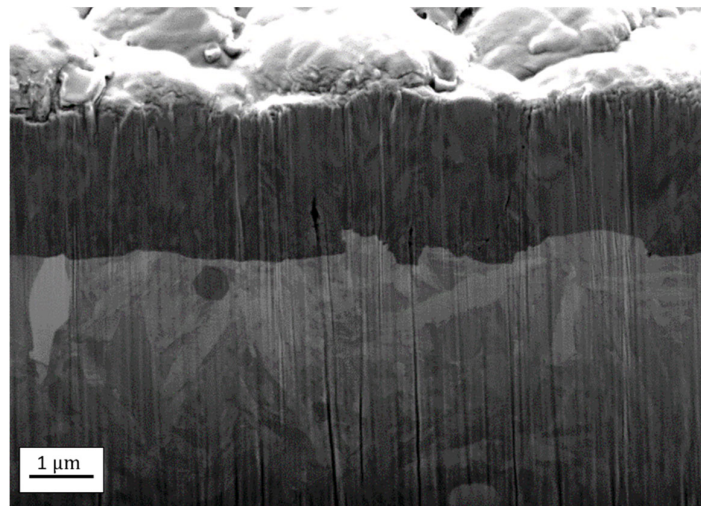
In this study two different types of testing were carried out using micro-cantilevers. These were:

- Testing the cohesive strength of coatings using micro-cantilevers that had been fabricated with the test surface parallel to the surface of the coating. This was applied to a TiN coating with a thickness of about 3  $\mu\text{m}$ .
- Testing the interfacial strength of a coating with micro-cantilevers that were machined perpendicular to the sample surface such that the interface between the coating and the substrate is subjected to a tensile stress. This technique was applied to a 50  $\mu\text{m}$  thick W based coating. An attempt was also made to apply the same technique to thin coatings with a thickness of a few micrometres, but this was unsuccessful due to the limited thickness of the coatings relative to the necessary size of the cantilevers.

### 2.1 MATERIALS

The substrates for the samples that were tested were manufactured from heat treated ASP23 tool steel. The samples evaluated in this work were 20 x 20 x 5 mm in size. One flat face of these samples were polished to a metallographic finish. Some samples were coated by Wallwork Cambridge with the TiN coating, and some were coated with a tungsten based composite CVD coating by Hardide Ltd with a coating with a thickness of about 50  $\mu\text{m}$ .

The TiN coating was approximately 2  $\mu\text{m}$  thick, shown in Figure 3, which shows a FIB cross-section through the coating and top of the substrate.



**Figure 3: Secondary electron image of a FIB cross-section through the TiN coating (dark contrast layer) and top of substrate (medium contrast bottom layer).**

For the W based coating, a cross section was made across the coating and substrate which was polished to a good finish. Secondary electron images were taken with a Zeiss Auriga 60 FIB-SEM with a 3 kV accelerating voltage, 60  $\mu\text{m}$  aperture and using the In-Lens detector. The steel substrate is at the bottom of the image in Figure 4, there is an interface layer on

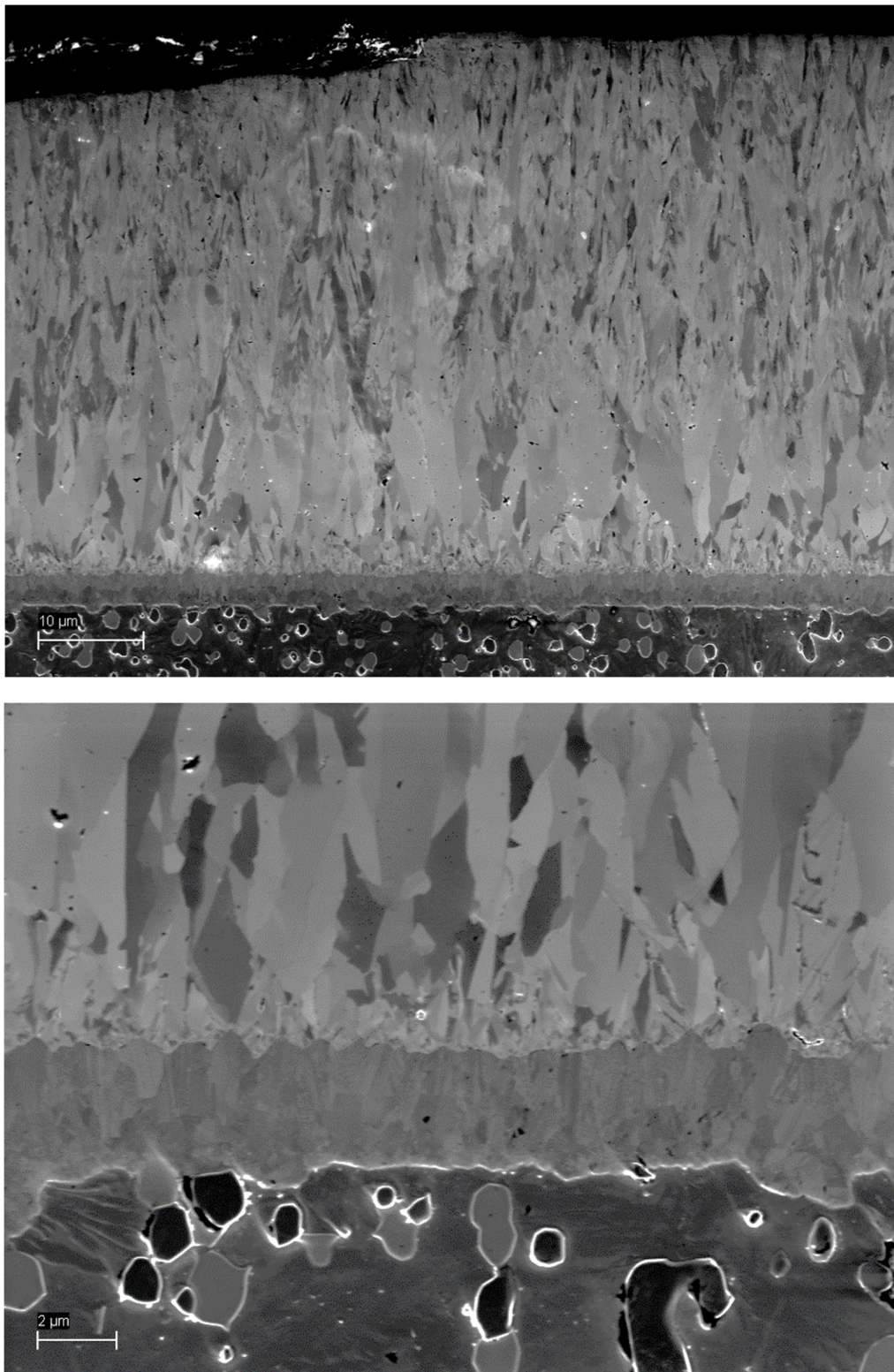
top of the substrate and then coating is above. The substrate has the darkest contrast and contains several different carbide phases. The interlayer is the dark grey contrast and a fine grain structure can be seen. The coating has the lightest contrast and contains a highly contrasted grain structure of varying sizes, where the coating has a fine grain structure near the interlayer, then large elongated grains on top (~10  $\mu\text{m}$  in length), then finer elongated grains in approximately the remaining two thirds of the coating.

After polishing and breaking out of the mount, the coating had cracked near the corner of the sample. Figure 5 shows an electron image of the crack where it runs along part of the interlayer-coating interface and through the entire thickness of the coating. The majority of the length of the crack runs along the grain boundaries in the coating.

Energy dispersive X-ray spectrometry (EDX) of the W based coating was carried out at 10 kV of the whole area shown in Figures 6 and 8, where the substrate is now at the top of the image (cyan), the interlayer beneath (magenta) and the coating below that (yellow). The substrate contains V and Cr, so these are likely the carbides that are visible, and the interlayer contains Ni. The coating contains W and C. Another area was mapped with only the coating (Spectrum 2 in Figure 7), where the proportion of W and C were 90% and 9% respectively in wt% and 38% and 58% respectively in at% (Figure 7). X-ray elemental maps were also produced and are shown in Figure 8.

Electron back scattered diffraction (EBSD) was performed at 30 kV accelerating voltage with a 60  $\mu\text{m}$  aperture of the W based coating. The Ni interlayer and some VC in the substrate indexed as fcc. The coating patterns matched a bcc structure, so W bcc phase was used to index as many points as possible. No WxCx phases were identified in the coatings.

The EBSD map confirmed the fine grain structure boundaries in the interlayer and in the coating next to the interlayer (Figure 9). There was good indexing of the large grains in the coating, however some indexing was missing on areas inside some grains, implying twinning or the presence of another phase. The band contrast (Figure 9b) also shows poor pattern quality in these regions, and there is a decrease in pattern quality and indexing towards the outer surface of the coating as the grains decrease in size. The Ni interlayer does not have any texture, but there is a strong texture of (001) in the W coating in the build direction (Figure 10).



**Figure 4: Electron images of the coating, interlayer and substrate**



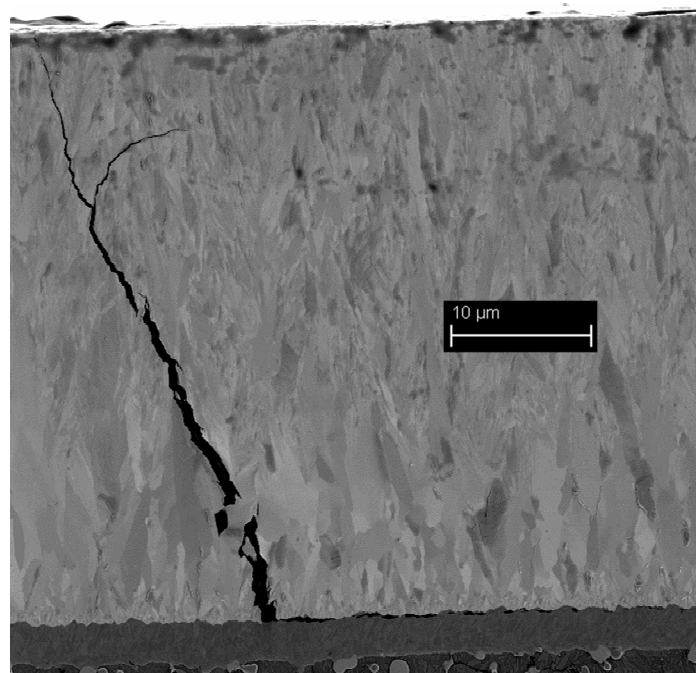


Figure 5: Electron image of crack through coating

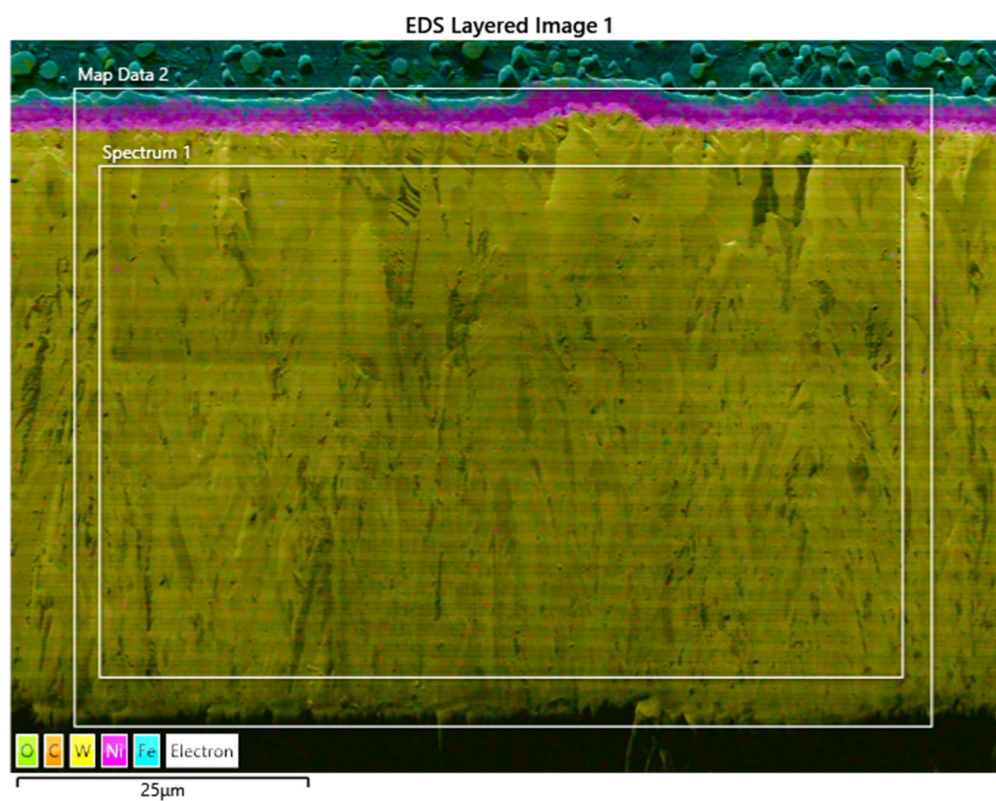


Figure 6: Area mapped with EDX and EBSD. Spectrum 1: EDX; Map Data 2: EBSD.

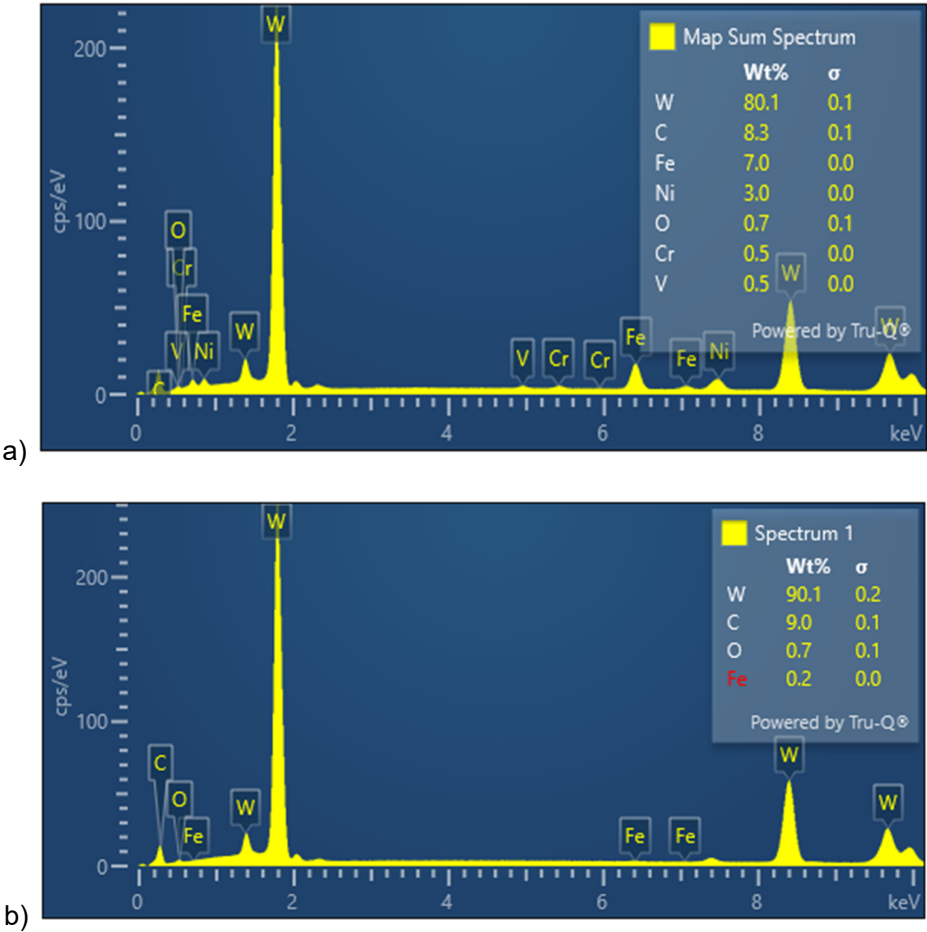
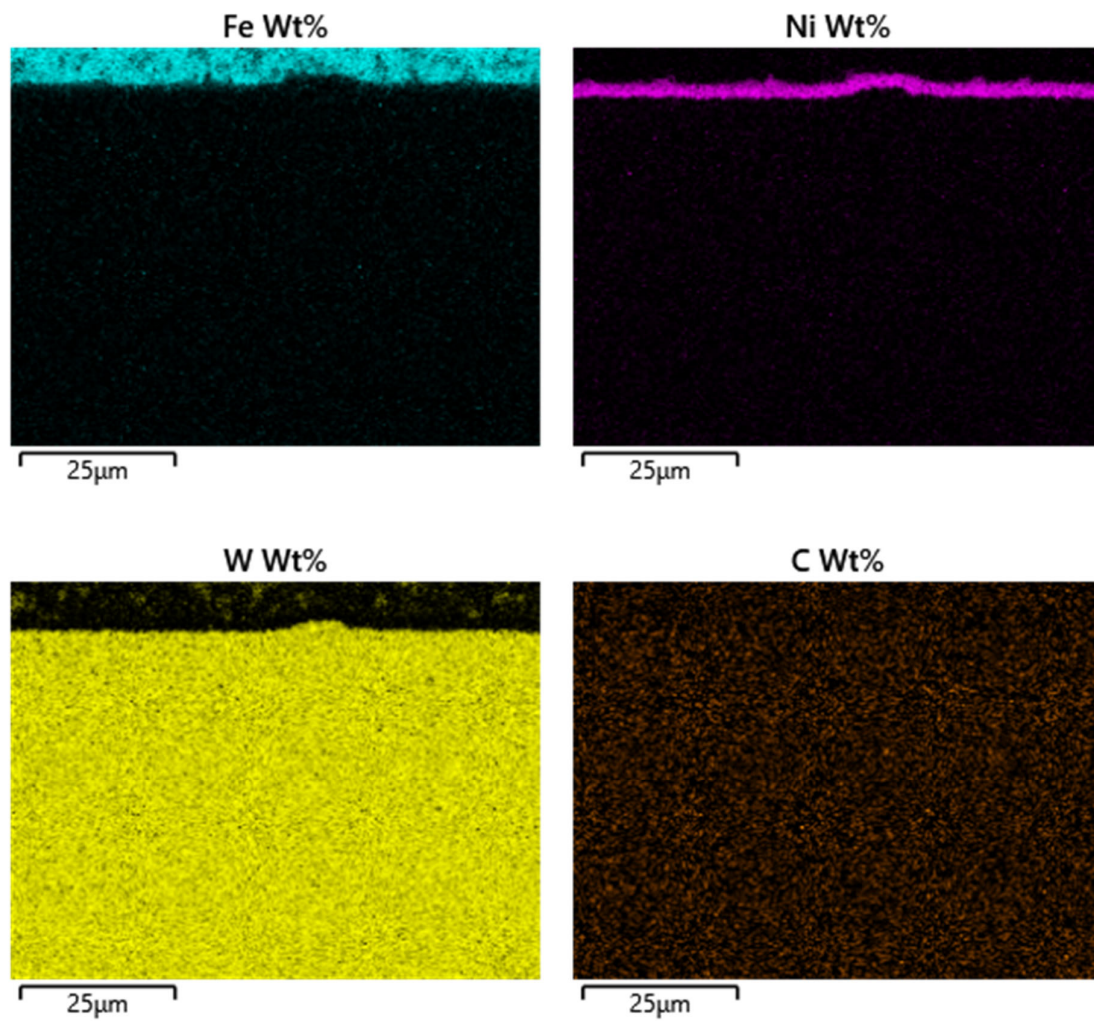
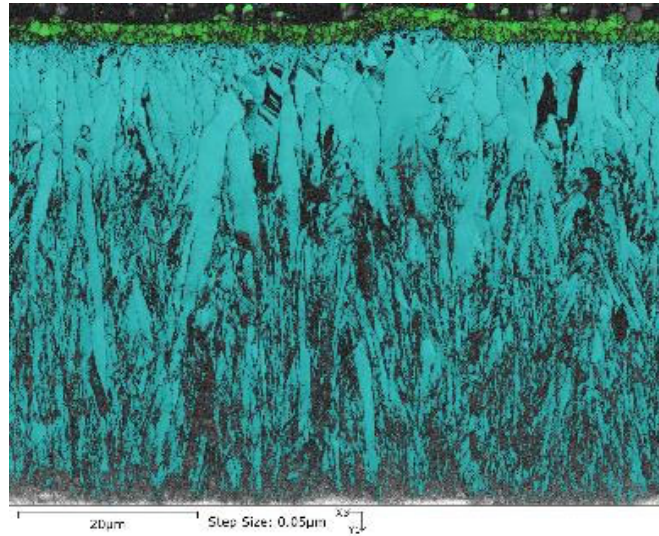


Figure 7: EDX spectra of areas in Figure 3. a) whole area, b) coating only

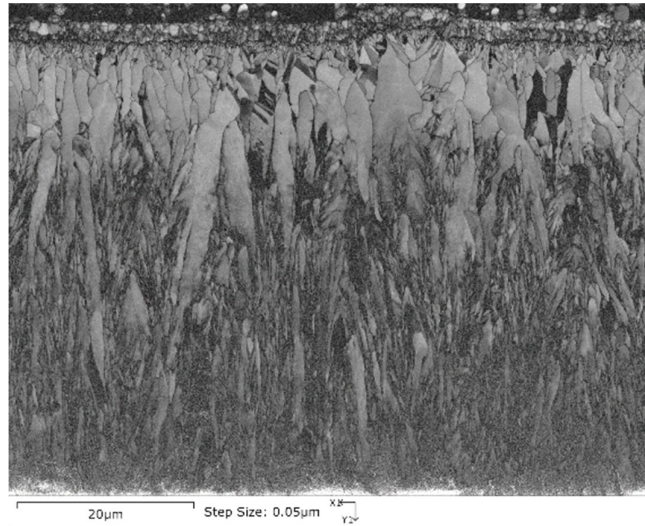


**Figure 8: Normalised EDX element maps**

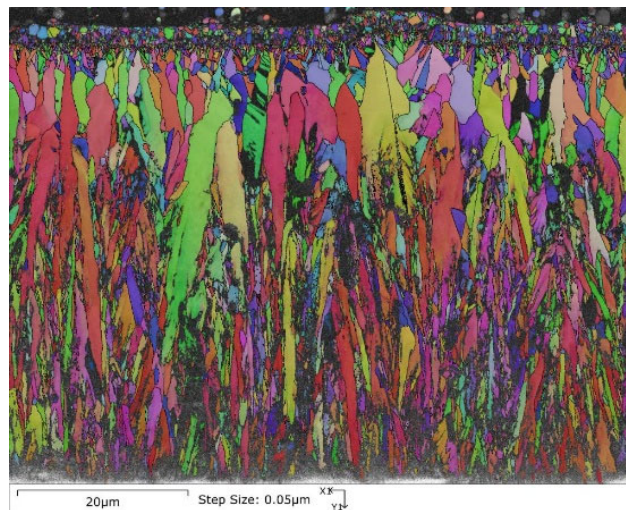




a)

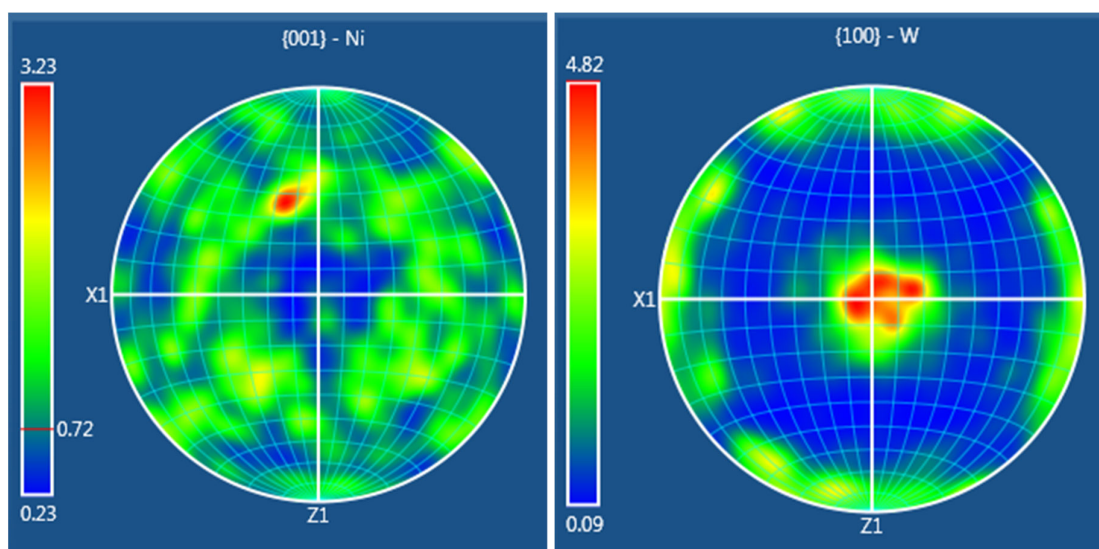


b)



c)

**Figure 9: EBSD maps showing a) phase, b) band contrast, and c) orientation (IPF colouring)**

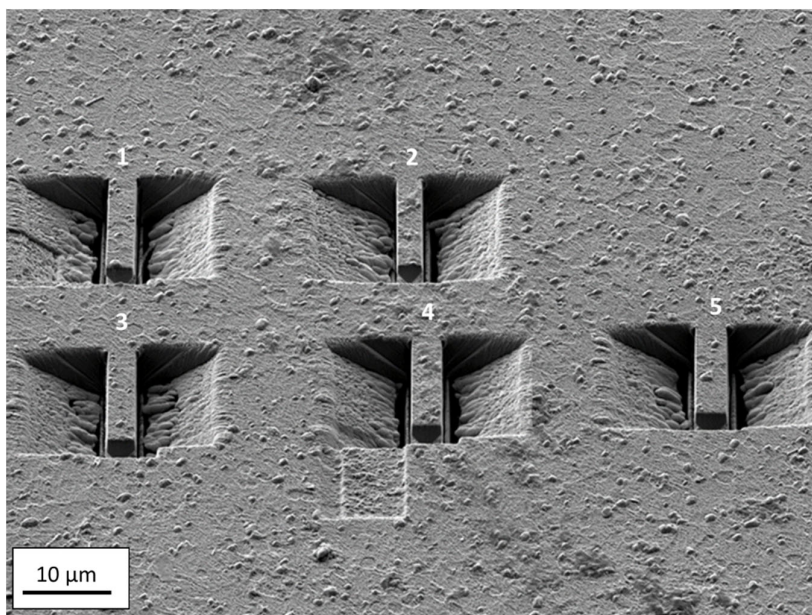


**Figure 10: Pole figures for Ni (interlayer) and W (coating) phases**

## 2.2 FIB MICROCANTILEVER FABRICATION

### 2.2.1 TiN cohesive strength cantilever

Cantilever beams were fabricated using a Zeiss Auriga 60 FIB-SEM, which is a gallium FIB, with a target geometry of 3  $\mu\text{m}$  in width, 12  $\mu\text{m}$  length, 1  $\mu\text{m}$  in height on the vertical edge and a triangular undercut at approximately 45°. Figure 11 shows five cantilevers, where the variation in geometry between them can be seen, despite using the same fabrication recipe.



**Figure 11: Micromechanical cantilevers machined in surface of TiN coating. Numbers refer to the test number.**

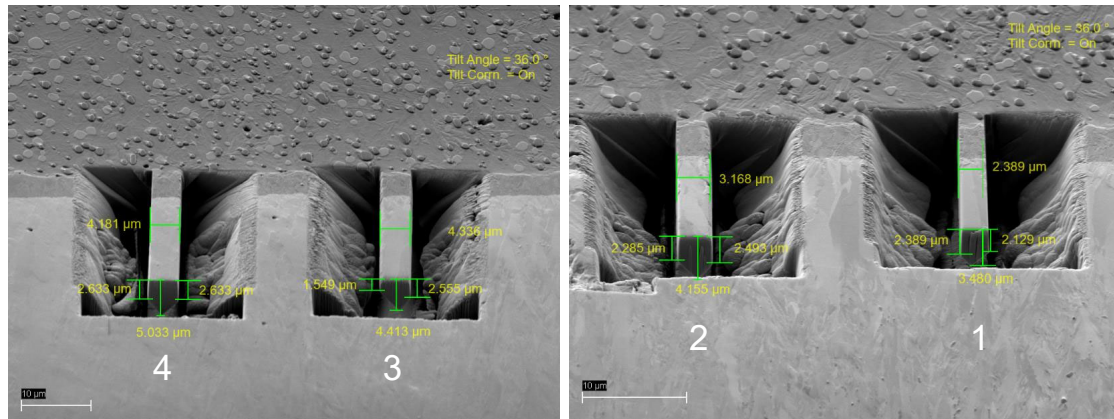


### 2.2.2 W based coating interface strength cantilever samples

These cantilevers were positioned with the substrate interface at the base and the interlayer interface further up the cantilevers, to increase the likelihood of failure along the interface under compression. The target width was 4  $\mu\text{m}$  with a length to width ratio of at least 4 to 1. A pentagonal cross-section shape was created, as they were produced in the bulk top surface of the coating. The geometry of the cantilevers were not exactly reproducible due to variability in the FIB technique. Table 1 and Figure 12 show the details of the cantilevers, where number 4 was tested several times.

**Table 1: Dimensions of cantilevers for W based coating**

| Test number                               | 1    | 2    | 3    | 4-1  | 4-2  | 4-3  |
|-------------------------------------------|------|------|------|------|------|------|
| Cantilever width ( $\mu\text{m}$ )        | 2.39 | 3.17 | 4.34 | 4.18 | 4.18 | 4.18 |
| Indenter position (length $\mu\text{m}$ ) | 12.0 | 15.9 | 21.7 | 20.9 | 16.7 | 16.7 |
| L:w ratio                                 | 5:1  | 5:1  | 5:1  | 5:1  | 4:1  | 4:1  |
| h/w                                       | 1.5  | 1.3  | 1.0  | 1.2  | 1.2  | 1.2  |
| Loading rate (nm/s)                       | -    | 10   | 10   | 10   | 10   | 50   |



**Figure 12: SEM images of cantilevers from W based coating labelled 1 to 4 with annotated measurements of height and width.**

### 2.3 MICROCANTILEVER TESTING

For the imaging and testing, the cantilever sample was mounted vertically opposite a conical/spherical 90° tip indenter. The nanoindenter was an ASMEC UNAT-SEM2 mounted inside a Zeiss Auriga 60 FIB-SEM, with the stage tilted at 20°. The electron beam imaged the cantilevers during testing with conditions of 5 kV accelerating voltage and a 30  $\mu\text{m}$  aperture.

The bend testing was displacement-controlled with a loading rate of 10 nm/s and unloading rate 20 nm/s, manually controlled until the cantilever had undergone some plastic behaviour or touched the bottom of the trench underneath. Figure 13 shows one of the TiN cantilever samples with the indenter just touching the end of the cantilever as the test is started.

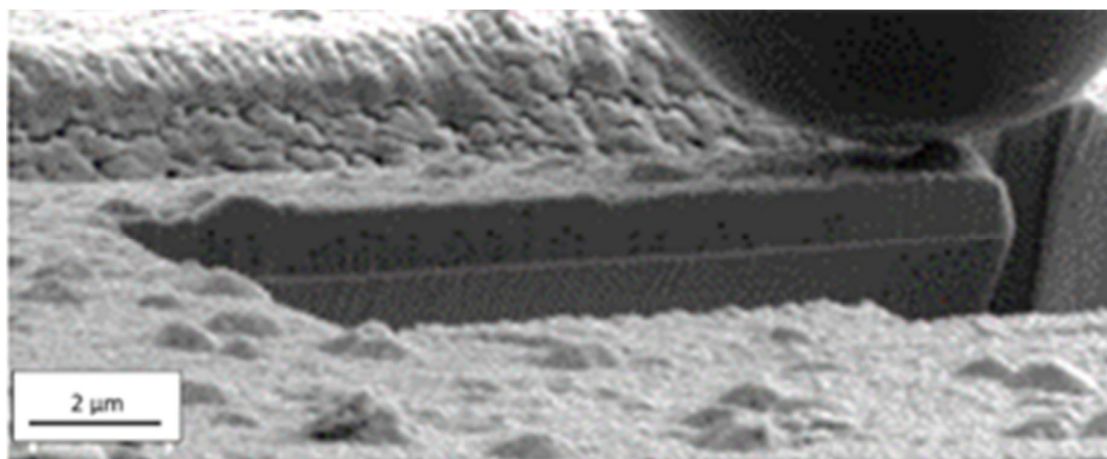


Figure 13: A cantilever (test 1) with the indenter aligned, just before the bend test commenced.

### 3 RESULTS

#### 3.1 TIN COHESIVE STRENGTH CANTILEVERS

The imaging of the tests showed that the cantilevers fractured between 1 and 2 μm from the base of the cantilever. Figure 14 shows a frame from the movie of one of the tests at the point of fracture. The crack can be seen in the SEM image at the same time as the load suddenly dropped at approximately 0.55 mN. All the failures occurred consistently vertically straight through the coating but were not straight on the top surface of the coating. The cracks differ in width between tests and the cracks on the top surface follow different paths. These differences will be due to the different local microstructures in each cantilever at the point of fracture as well slight differences in geometry between the cantilevers.

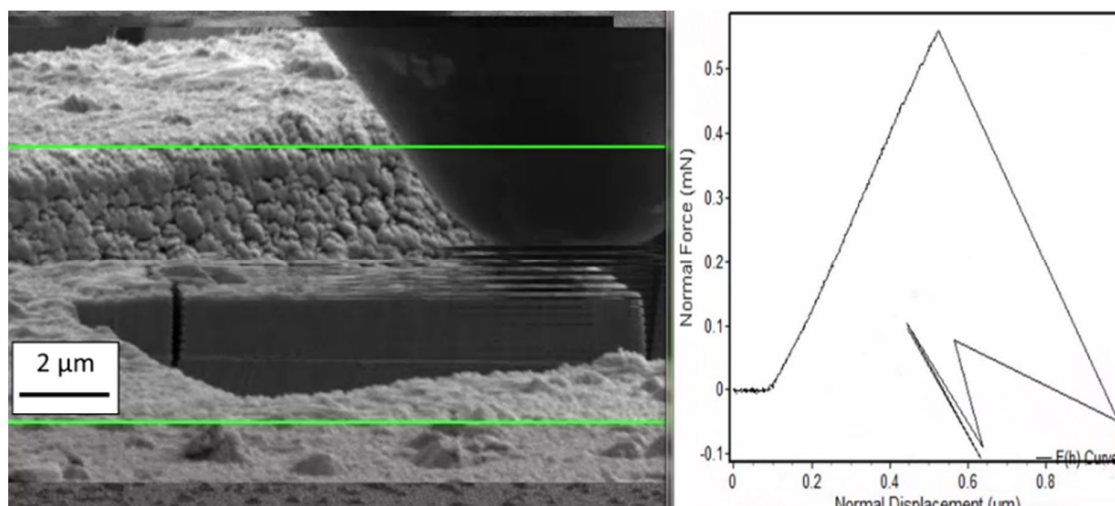
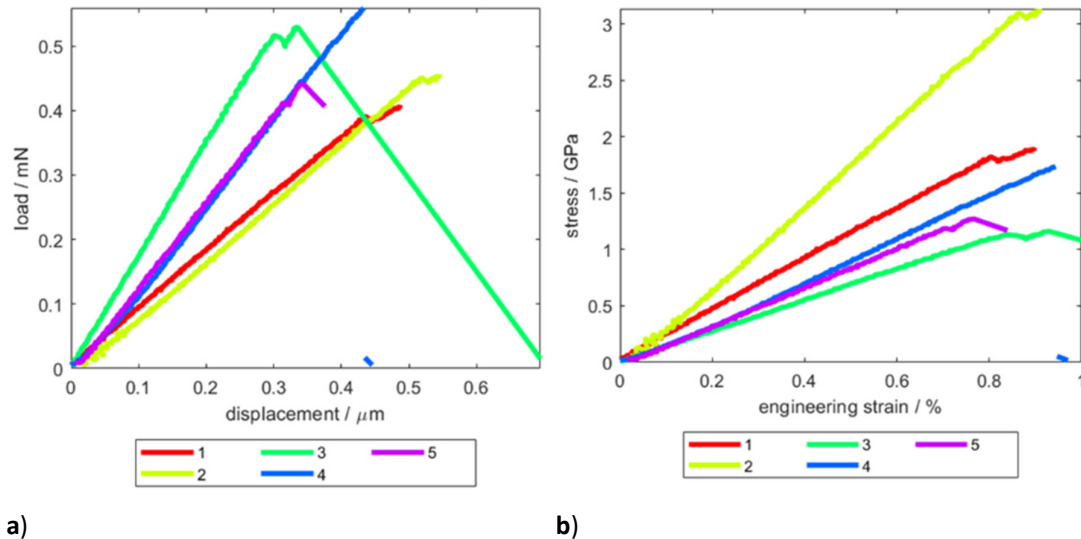


Figure 14, SEM image and mechanical data in a movie frame at point of fracture of a cantilever (test 4). The horizontal lines beneath the indenter are image artefacts where the indenter is vibrating quickly just after the fracture and being imaged intermittently during the slower image scanning.

The load-displacement data from the five tests were plotted in Figure 15a. The fracture loads were between 0.4 and 0.55 mN for the tests. The stress and strain were calculated using the measured geometries of each cantilever and the load-displacement data. The loading portion of the curves are plotted in Figure 15b as stress against engineering strain. Technically, the elastic modulus could be calculated from the gradient of the curves in Figure 22b; the results are scattered, and the range of values is approximately between 180 and 380 GPa.



a) b)  
**Figure 15: Graphs of five bend tests of the cantilever beams in Figure 3. a) Load-displacement data, b) stress and engineering strain data.**

### 3.2 W BASED INTERFACE STRENGTH CANTILEVERS

Table 2 contains observations of the cantilever behaviour during the test and images after the test. It was found that plastic deformation occurred earlier (at lower load) in test 2. This test also showed the steepest rate of increase of load in the test, indicating the highest elastic modulus. This test was the only one where failure occurred at the interface


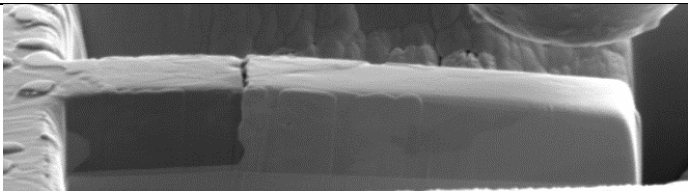
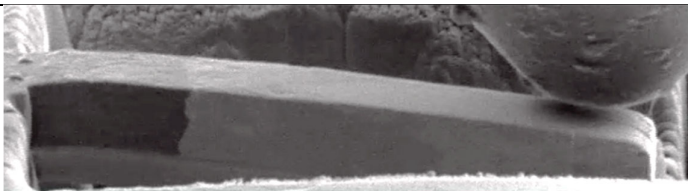
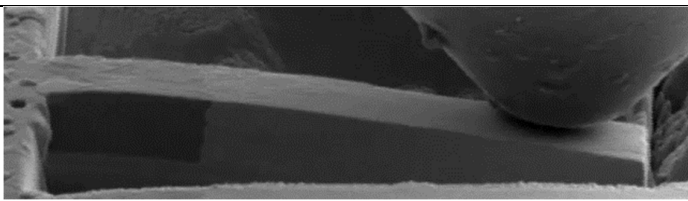
The load-displacement data, shown in Figure 16, from the bend test and the geometry of the cantilevers were used to calculate stress and strain, shown in Figure 17. The three repeats on cantilever 4 were plotted on the same graphs. The inset graphs show the differentials of the stress-strain curves with respect to strain. The value of the nearly flat part of these curves gives an indication of the elastic behaviour of the cantilevers.

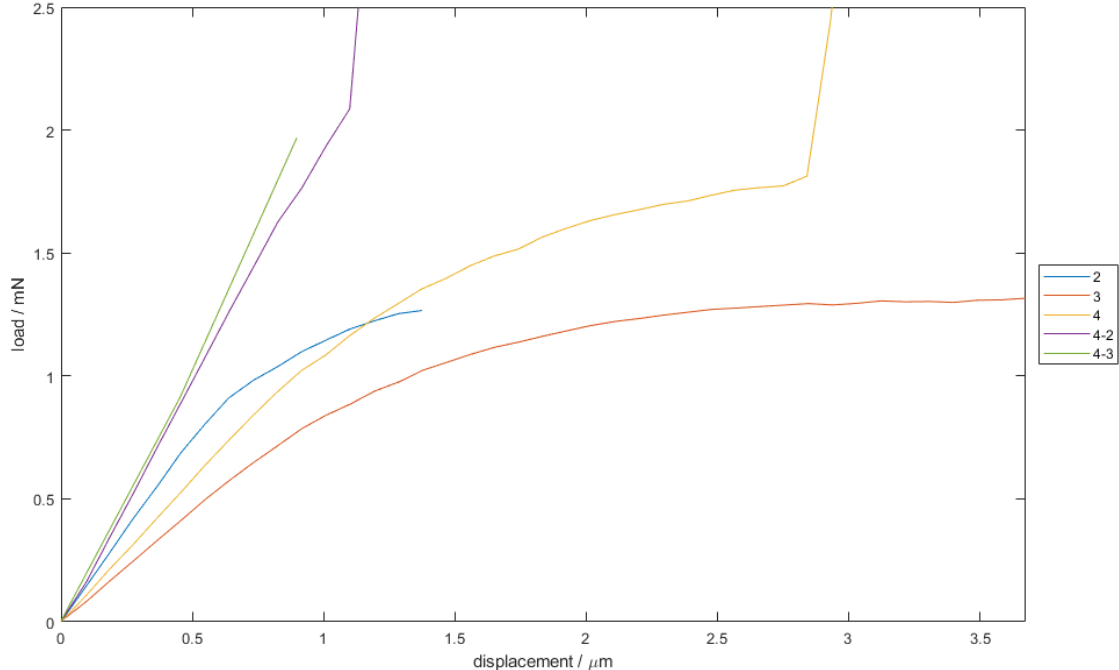
## 4 DISCUSSION

Although cantilever samples have been successfully fabricated and tested, several practical drawbacks with the approach have been shown. Firstly, it is complex and time consuming to manufacture the cantilever samples from the coating systems. Careful planning and a complex series of micromachining steps are required to produce the samples. Combined with the low machining rate of a gallium ion FIB this means that it takes several days to produce a set of cantilevers. There is also a trade off between the quality of the micromachining and the speed. A lack of repeatability in the micromachining means that the although the production of identical cantilevers is intended differences in processing and materials response from cantilever mean that there is a significant variation in finished cantilever geometries as seen in Table 1.

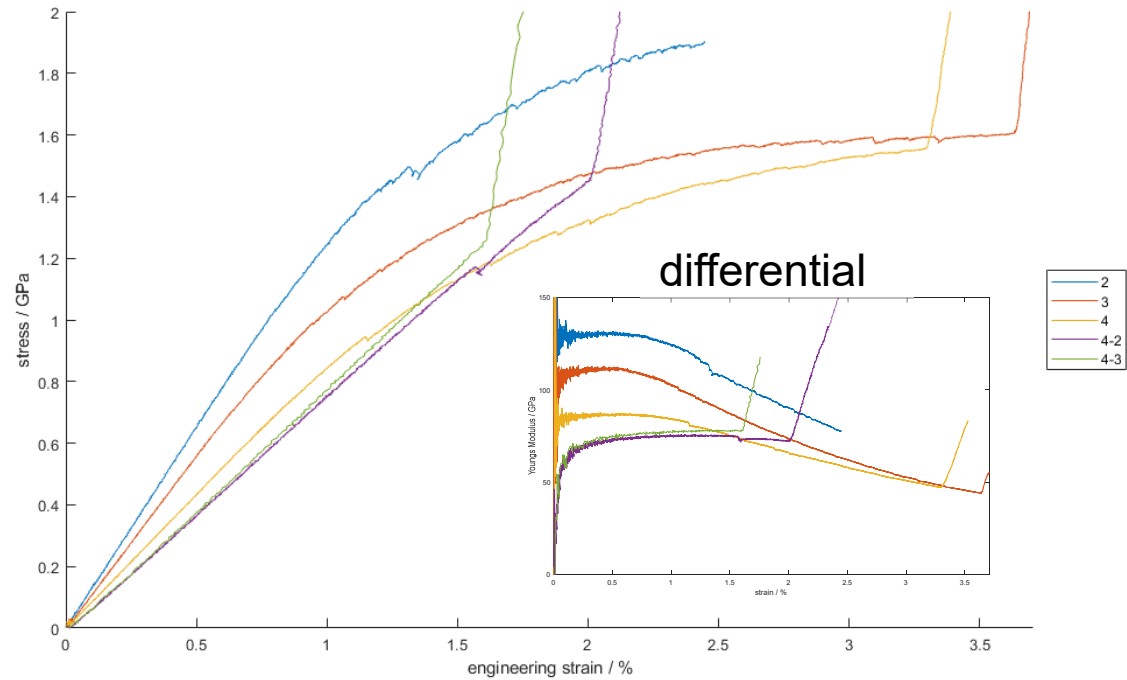
Secondly, the small scale of the samples means that inevitably the testing is sensitive to the point to point variations in the makeup and structure of the materials being tested. Thus the scale of the samples is not that much larger than the scale of the microstructures of the materials systems under examination, so that the presence of, for example, a large carbide particle in the substrate near the interface of a large grain in the coating may cause statistical variations in the test results.

**Table 2: Observations during and after testing**

| Test number | Notes                                                                                                                                                                                                                       | Image after test                                                                     |
|-------------|-----------------------------------------------------------------------------------------------------------------------------------------------------------------------------------------------------------------------------|--------------------------------------------------------------------------------------|
| 1           | Indenter jolted at beginning of test and failed the cantilever. Indenter impression was made on the top surface. Cantilever plastically deformed, no cracks observed.                                                       |    |
| 2           | Cracked at W-Ni interface                                                                                                                                                                                                   |    |
| 3           | Did not fail, slight plastic deformation (did not return to original position). Appeared to bend most at substrate-Ni interface, and Ni-W interface remained straight                                                       |  |
| 4           | Similar to test 3<br><br>2 <sup>nd</sup> repeat: Did not behave differently to first test on this cantilever, just started from slightly pre-bent position<br><br>3 <sup>rd</sup> repeat: similar to 2 <sup>nd</sup> repeat |  |



**Figure 16: Load-displacement curves for the cantilever tests**



**Figure 17: Stress-strain curves for the cantilever tests, with an inset graph of the differentials of the curves.**

These two factors (variation in sample size and microstructural effects) are likely to be the reason for the variation in results that is observed with the difference in the load-displacement curves that were obtained in both types of test. When the measurement of

sample geometry is taken into account to calculate stress-strain curves the variation in results is reduced. Nevertheless, some variation remains which is likely to be due to the microstructural factors. This situation is similar to the statistical variation due to microstructural effects in the strength testing of brittle materials such as ceramics. For ceramics it is normal to test a relatively large number of samples (at least 10 up to 30) to understand this statistical variation in samples.

For the samples in the W based samples it is interesting that only one of the samples had any failure at the coating interface, with the rest of the samples undergoing plastic deformation. The tests where there was no failure were only stopped when the bend in the sample had become so large that the end of the sample was in danger of touching the base of the trench.

Moving forward it is intended to focus any continuing work on optimising the fabrication conditions to enable the production of larger sets of samples to enable microstructural factors to be taken into account by increasing number of tests. Another focus will be to develop micromechanical tests that can be used to test the interfacial strength for thin coatings with a thickness of a few micrometres.

## **5 CONCLUSIONS**

Cantilever samples were successfully produced in a thin TIN coating for cohesive strength testing of the coatings, and in a W based coating for interface testing. It was found that there was variation in the test results that came from the variation in cantilever geometry due to micromachining and microstructural effects.

Most of the tests on the W based coating showed no failure at the interface between the coating and the substrate. One test showed some interface failure, but even in this case total failure of the sample did not occur.

## **6 ACKNOWLEDGEMENTS**

The authors would like to thank the Department of Science Innovation and Technology for funding from the National Measurement System.

## **7 REFERENCES**

- 1) Mingard, K P; Cox, D C; Jones, H G; Gee, M G (2016) The use of focused ion beam microscopy for 3D material characterisation. Measurement Good Practice Guide. 141
- 2) Igaki, J. Y., Nakamatsu, K. I., Kometani, R., Kanda, K., Haruyama, Y., Kaito, T., & Matsui, S. (2006). Mechanical characteristics and applications of diamondlike-carbon cantilevers fabricated by focused-ion-beam chemical vapor deposition. *Journal of Vacuum Science and Technology B: Microelectronics and Nanometer Structures*, 24(6), 2911–2914. <https://doi.org/10.1116/1.2357960>
- 3) Liu, D., & Flewitt, P. E. J. (2012). The Measurement of Mechanical Properties of Thermal Barrier Coatings by Micro-Cantilever Tests. *Key Engineering Materials*, 525–526, 13–16. <https://doi.org/10.4028/www.scientific.net/KEM.525-526.13>
- 4) Y Chen, X Zhang, X Zhao, N Markocsan, P Nylén, Ping Xiao, Measurements of elastic modulus and fracture toughness of an air plasma sprayed thermal barrier coating using micro-cantilever bending, *Surface & Coatings Technology* 374 (2019) 12–20

- 5) Robertson, A. L., & White, K. W. (2017). Microscale fracture mechanisms of a Cr<sub>3</sub>C<sub>2</sub>-NiCr HVOF coating. *Materials Science and Engineering: A*, 688, 62–69.  
<https://doi.org/10.1016/j.msea.2017.01.097>
- 6) Best, J. P., Wehrs, J., Polyakov, M., Morstein, M., & Michler, J. (2019). High temperature fracture toughness of ceramic coatings evaluated using micro-pillar splitting. *Scripta Materialia*, 162, 190–194.  
<https://doi.org/10.1016/j.scriptamat.2018.11.013>
- 7) Sebastiani, M., Johannis, K. E., Herbert, E. G., Carassiti, F., & Pharr, G. M. (2015). A novel pillar indentation splitting test for measuring fracture toughness of thin ceramic coatings. *Philosophical Magazine*, 95(16–18), 1928–1944.  
<https://doi.org/10.1080/14786435.2014.913110>
- 8) Mu, Y., Zhang, X., Hutchinson, J. W., & Meng, W. J. (2017). Measuring critical stress for shear failure of interfacial regions in coating/interlayer/substrate systems through a micro-pillar testing protocol. *Journal of Materials Research*, 32(8), 1421–1431.  
<https://doi.org/10.1557/jmr.2016.516>
- 9) I El Azhari, J Garcia, M Zamanzade, F Soldera, C Pauly, L Llanes, F Mucklich, Investigations on micro-mechanical properties of polycrystalline Ti(C,N) and Zr(C,N) coatings, *Acta Materialia* 149(2018), doi: 10.1016/j.actamat.2018.02.053